

Energy and angular distributions of the bottom quark in the electron–positron annihilation $e^+e^- \rightarrow bW^+\bar{t}$

I.V. Truten ^{1,*}, A.Yu. Korchin ^{1,2,†}

¹*NSC “Kharkov Institute of Physics and Technology”, 61108 Kharkiv, Ukraine*

²*V.N. Karazin Kharkiv National University, 61022 Kharkiv, Ukraine*

**i.truten@kipt.kharkov.ua*

†korchin@kipt.kharkov.ua

Received 10 September 2020

Revised 24 October 2020

Accepted 24 November 2020

Published 26 January 2021

The distributions of the bottom quark in the process $e^+e^- \rightarrow t\bar{t} \rightarrow bW^+\bar{t}$ are considered at the e^+e^- energy corresponding to the first construction stage of the Compact Linear Collider. The cross-sections of $e^+e^- \rightarrow t\bar{t} \rightarrow bW^+\bar{t}$, as functions of the b -quark energy and angle with respect to the direction of the electron beam, are derived and calculated. The effects of physics beyond the Standard Model are included via the modified $\gamma t\bar{t}$ and $Zt\bar{t}$ couplings which naturally appear in effective field theories. In addition to the cross-sections, the energy and angular asymmetries are calculated. The dependence of these observables on the e^+e^- energy is calculated, and features of this dependence are investigated.

Keywords: Bottom quark; top quark; energy and angular distributions; electron–positron annihilation

PACS numbers: 12.15.-y, 12.60.-i, 14.65.Fy, 14.65.Ha

1. Introduction

Nowadays the global interest in particle physics is the search for “new physics”, or physics beyond the Standard Model (SM). An important direction of research is study of properties of the top quark. These properties are planned to be explored precisely on future electron–positron colliders, such as International Linear Collider (ILC)¹ and Compact Linear Collider (CLIC).^{2–4} The ILC will start at the center-of-mass (CM) energy of 250 GeV followed by 500 GeV upgrade.^{4,5} The CLIC promises to be a good candidate for production of the on-mass-shell top quark and studying its properties. At the first construction stage of the CLIC, the CM energy will be

[†]Corresponding author

380 GeV with expected integrated luminosity of 1 ab^{-1} , which will include 100 fb^{-1} collected near the $t\bar{t}$ production threshold.^{3,4,6}

This work is a continuation of our previous paper,⁷ where the polarization of the top quark, produced in electron–positron annihilation, was studied in detail with emphasis on physics beyond the SM (BSM). The aim of the present paper is to consider the consequent decay of the top quark $e^+e^- \rightarrow t\bar{t} \rightarrow bW^+\bar{t}$. Clearly, the observables related to the bottom quark are more appropriate for the future experimental investigations.

Note that this reaction was studied in Refs. 8–11, where the distributions of the lepton, coming from the decay $W^+ \rightarrow \ell^+\nu_\ell$, were evaluated. The issue of a possible CP violation was studied. CP violation in framework of the MSSM was discussed and estimated in the spectra of the bottom quark in Refs. 12–15.

In this paper, we concentrate on distributions of the bottom quark. In addition to the SM, we take into account the BSM effects which are described by the anomalous interactions of the photon and Z boson with the top quark. These interactions naturally appear in effective field theory (EFT) Lagrangian (see, e.g., Ref. 16), which contains both the SM Lagrangian and the higher-dimensional terms beyond the SM. The calculations in our paper are performed using the formalism developed in Ref. 17 which allows one to find in a compact form distributions of the secondary particles, such as the bottom quark in $e^+e^- \rightarrow t\bar{t} \rightarrow bW^+\bar{t}$.

We investigate effects of the BSM couplings κ and κ_z , which determine the anomalous $\gamma t\bar{t}$ and $Z t\bar{t}$ vertices, and influence of the polarization of the top quark arising in the $e^+e^- \rightarrow t\bar{t}$ process on the energy and angular distributions of the b quark. In this connection note, that in framework of the SM, the distribution of the bottom quark was analytically derived in Ref. 9 for the unpolarized leptons and in Ref. 18 for the longitudinally polarized leptons. In this work we perform calculation beyond the SM, where analytical consideration is rather cumbersome, and using the formalism¹⁷ facilitates calculations.

The structure of the paper is as follows. In Section 2 theoretical basis for calculation of the process $e^+e^- \rightarrow t\bar{t} \rightarrow bW^+\bar{t}$ is overviewed. Two possible ways of calculation of the cross-section suggested in Ref. 17 are mentioned. We also introduce polarization vector of the top quark which arises in the production process $e^+e^- \rightarrow t\bar{t}$.⁷ In Subsection 2.1 the cross-section of $e^+e^- \rightarrow bW^+\bar{t}$ is considered as a function of the bottom-quark energy E_b , while in Subsection 2.2 the cross-section is obtained as a function of the polar angle θ_b between the momentum of b quark and direction of electron beam. In Section 3 results of calculation in the SM and BSM of the $e^+e^- \rightarrow bW^+\bar{t}$ cross-sections as functions of the energy E_b and the angle θ_b are presented. The BSM results are obtained for some values of the coupling constants κ and κ_z . Several observables, such as normalized energy and angle distributions, and energy and angular asymmetries are studied at various values of κ and κ_z . Dependence of asymmetries on the e^+e^- invariant energy is investigated. In Section 4 conclusions are given. Appendix A contains a proof of the gauge in-

variance of the photon-exchange diagram for the process $e^+e^- \rightarrow t\bar{t} \rightarrow bW^+\bar{t}$ in the narrow-width approximation.

2. Formalism for the Process $e^+e^- \rightarrow bW^+\bar{t}$

Let us consider electron–positron annihilation into a pair of top quarks, where one of the quarks decays, $t \rightarrow bW^+$, *i.e.* the process $e^+e^- \rightarrow t\bar{t} \rightarrow bW^+\bar{t}$. To calculate the energy and the angular distribution of the b quark one can use efficient formalism of Refs. 8, 17. According to these papers there are two equivalent ways of calculation of the cross-section of interest. In the first way the cross-section is written as

$$d\sigma(e^+e^- \rightarrow bW^+\bar{t}) = \int \frac{d\sigma(e^+e^- \rightarrow t\bar{t}; 0)}{d\Omega_t} \frac{d\Gamma(t \rightarrow bW^+; a^\mu)}{\Gamma_t} d\Omega_t, \quad (1)$$

where $d\sigma(e^+e^- \rightarrow t\bar{t}; 0)/d\Omega_t$ is the differential cross-section of the electron–positron annihilation to the top quarks, which is calculated for all unpolarized particles. $d\Gamma(t \rightarrow bW^+; a^\mu)$ is the differential width of the decay of the polarized top quark, where its polarization arises in the process $e^+e^- \rightarrow t\bar{t}$ and is described by the four-vector a^μ . The cross-section is calculated in the CM frame, while the $t \rightarrow bW^+$ differential decay width and the total width Γ_t are evaluated in the top-quark rest frame.

The second way of calculation implies that the cross-section can be presented as

$$d\sigma(e^+e^- \rightarrow bW^+\bar{t}) = 2 \int \frac{d\sigma(e^+e^- \rightarrow t\bar{t}; n^\mu)}{d\Omega_t} \frac{d\Gamma(t \rightarrow bW^+; 0)}{\Gamma_t} d\Omega_t, \quad (2)$$

where the $e^+e^- \rightarrow t\bar{t}$ differential cross-section is calculated for the polarized top quark with the polarization four-vector n^μ

$$n^\mu = \alpha_b \left(\frac{p_b^\mu m_t}{p_t \cdot p_b} - \frac{p_t^\mu}{m_t} \right), \quad n \cdot p_t = 0, \quad n \cdot n = -\alpha_b^2, \quad (3)$$

where p_t^μ (p_b^μ) is the four-momentum of the top (bottom) quark, and the parameter α_b determines the asymmetry in the decay $t \rightarrow bW^+$ of the polarized top quark. Also in Eq. (2) $d\Gamma(t \rightarrow bW^+; 0) = \frac{1}{2} \sum_s d\Gamma^{(s)}$ is the initial spin-averaged differential decay width.

Below we will mainly use the form in Eq. (1), since only the $e^+e^- \rightarrow t\bar{t}$ unpolarized cross-section enters, while the polarization vector a^μ of the produced top quark was already calculated in Ref. 7. In Sec. 3 we check explicitly the equivalence of the cross-sections in Eqs. (1) and (2).

Let us discuss the distribution of the bottom quark. In general, the differential decay width of $t \rightarrow bW^+$ is

$$d\Gamma = \frac{1}{2m_t} |\mathcal{M}|^2 dX_{LIPS} \quad (4)$$

with dX_{LIPS} being the Lorentz invariant phase space, and the matrix element squared for the polarized top quark and the unpolarized W boson and b quark

reads

$$|\mathcal{M}|^2 = \sqrt{2} G_F N |V_{tb}|^2 (1 + \alpha_b \vec{P} \vec{n}_{b,R}) = \sqrt{2} G_F N |V_{tb}|^2 \left(1 - \alpha_b \frac{m_t a \cdot p_b}{p_t \cdot p_b} \right), \quad (5)$$

where G_F is the Fermi weak constant, $V_{tb} \approx 1$ is the element of the CKM matrix, and

$$N = (m_t^2 - m_W^2)(2m_W^2 + m_t^2), \quad \alpha_b = \frac{2m_W^2 - m_t^2}{2m_W^2 + m_t^2} = -0.40. \quad (6)$$

Here m_t (m_W) is the mass of the top quark (W boson) and we neglect the bottom-quark mass, *i.e.* put $m_b = 0$. Note that Eq. (5) is written both in the rest frame of the top quark (denoted by the subscript ‘‘R’’) and in the Lorentz-invariant form. In the frame ‘‘R’’, $\vec{n}_{b,R}$ is the unit vector in the direction of the b -quark momentum, and the t -quark polarization is determined by the three-vector \vec{P} , such that $a_R^\mu = (0, \vec{P})$. In the frame, where t quark moves with the momentum \vec{p}_t and energy E_t , the polarization four-vector is¹⁹

$$a^\mu = \left(\frac{\vec{P} \vec{p}_t}{m_t}, \vec{P} + \frac{\vec{p}_t (\vec{P} \vec{p}_t)}{m_t (m_t + E_t)} \right), \quad a \cdot p_t = 0, \quad a \cdot a = -\vec{P}^2. \quad (7)$$

The total decay width is

$$\Gamma_t = \frac{p_b^0 G_F |V_{tb}|^2 N}{4\sqrt{2}\pi m_t^2}, \quad (8)$$

where $p_b^0 = (m_t^2 - m_W^2)/2m_t$ is the bottom-quark momentum (energy) in the t -quark rest frame.

The two-particle phase space,

$$dX_{LIPS} = (2\pi)^4 \delta^4(p_t - p_b - p_W) \frac{d^3 p_b}{(2\pi)^3 2E_b} \frac{d^3 p_W}{(2\pi)^3 2E_W}, \quad (9)$$

where E_b and E_W is the energy of the bottom quark and W boson, respectively, allows one to integrate over the W -boson momentum and obtain

$$\begin{aligned} \frac{1}{\Gamma_t} d\Gamma(t \rightarrow b W^+, a^\mu) &= \frac{m_t}{4\pi p_b^0} \left(1 - \alpha_b \frac{m_t a \cdot p_b}{p_t \cdot p_b} \right) \\ &\times \delta(E_t - E_b - E_W) \frac{E_b}{E_W} dE_b d\Omega_b \end{aligned} \quad (10)$$

with $E_W = (m_W^2 + \vec{p}_t^2 + E_b^2 - 2\vec{p}_t \vec{p}_b)^{1/2}$ and $E_b = |\vec{p}_b|$. Substitution of (10) in (1) gives the required cross-section

$$\begin{aligned} d\sigma(e^+ e^- \rightarrow b W^+ \bar{t}) &= \frac{m_t}{4\pi p_b^0} \int \frac{d\sigma(e^+ e^- \rightarrow t\bar{t}; 0)}{d\Omega_t} \left(1 - \alpha_b \frac{m_t a \cdot p_b}{p_t \cdot p_b} \right) \\ &\times \delta(E_t - E_b - E_W) \frac{E_b}{E_W} dE_b d\Omega_b d\Omega_t, \end{aligned} \quad (11)$$

from which one can obtain the energy and angular distributions of the bottom quark for arbitrary $e^+ e^- \rightarrow t\bar{t}$ cross-section.

2.1. Energy spectrum of the bottom quark

For this case the coordinate system is chosen as shown in Fig. 1 (left): the top-quark (and antiquark) momentum is directed along the OZ' axis, the electron (and positron) momentum lies in the $X'OZ'$ plane, the bottom-quark momentum points in arbitrary direction. Further, θ_t is the angle between the electron and the top-quark momenta, θ'_b is the angle between \vec{p}_t and \vec{p}_b .

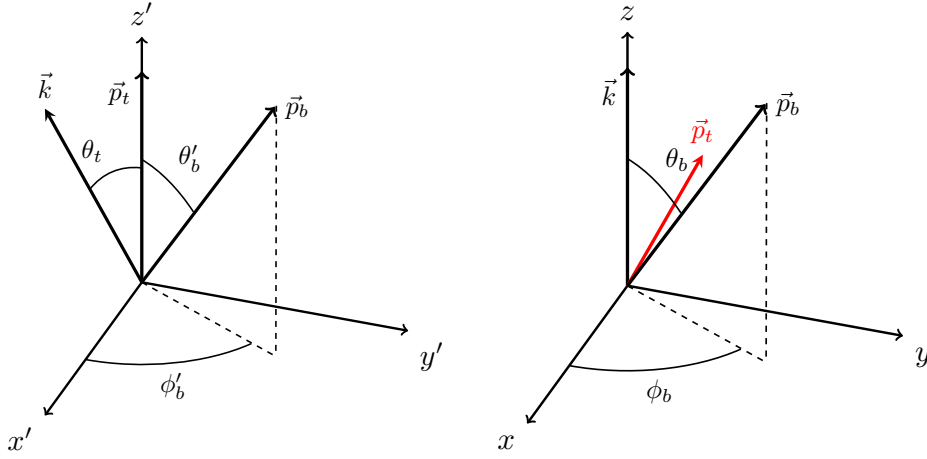


Fig. 1. The coordinate systems used for the energy distribution (left) and the angular distribution (right) of the bottom quark.

In the CM frame, the four-momenta of e^- , t and b quarks, and polarization vector are

$$\begin{aligned}
 k^\mu &= E_t(1, \sin \theta_t, 0, \cos \theta_t), \\
 p_t^\mu &= E_t(1, 0, 0, V), \\
 p_b^\mu &= E_b(1, \sin \theta'_b \cos \phi'_b, \sin \theta'_b \sin \phi'_b, \cos \theta'_b), \\
 a^\mu &= (\gamma V P_{z'}, P_{x'}, P_{y'}, \gamma P_{z'}),
 \end{aligned} \tag{12}$$

where $V = p_t/E_t$ is the velocity of the top quark, and $\gamma = E_t/m_t$ is the Lorentz factor. The components of the polarization vector $\vec{P} = (P_{x'}, P_{y'}, P_{z'})$ have been evaluated in Ref. 7 as functions of the top-quark angle θ_t . Then one can carry out integration in Eq. (11) over the angles of the b quark θ'_b and ϕ'_b , and the cross-section as a function of the bottom-quark energy becomes

$$\begin{aligned}
 \frac{d\sigma(e^+e^- \rightarrow bW^+\bar{t})}{dE_b} &= \frac{1}{2\gamma V p_b^0} \int_{-1}^{+1} \frac{d\sigma(e^+e^- \rightarrow t\bar{t}; 0)}{d\cos \theta_t} \\
 &\times \left[1 + \frac{\alpha_b P_{z'}(\theta_t)}{V} \left(\frac{E_b}{\gamma p_b^0} - 1 \right) \right] d\cos \theta_t,
 \end{aligned} \tag{13}$$

where the energy varies within the limits

$$E_- \leq E_b \leq E_+, \quad E_{\pm} = \frac{p_b^0}{\gamma(1 \mp V)}. \quad (14)$$

It is seen that only the longitudinal component of the quark polarization survives after integration over the azimuthal angle ϕ'_b . The cross-section in Eq. (13) is linear in the energy E_b , if we keep the polarization of the top quark. If polarization is neglected, *i.e.* $\vec{P} = 0$, the cross-section (13) is independent of the b -quark energy. In the SM, this feature was pointed out in Ref. 18, and apparently this is a general property of the energy spectrum regardless of a model for $e^+e^- \rightarrow t\bar{t}$. It is also interesting that the t -quark polarization does not contribute at the b -quark energy $\tilde{E}_b = \gamma p_b^0$, as is seen from the last term in (13).

Using Eq. (13) we can calculate the total cross-section by integrating (13) over E_b . Then use of (14) yields

$$\begin{aligned} & \int_{E_-}^{E_+} \frac{d\sigma(e^+e^- \rightarrow bW^+\bar{t})}{dE_b} dE_b \\ &= \int_{-1}^{+1} \frac{d\sigma(e^+e^- \rightarrow t\bar{t}; 0)}{d\cos\theta_t} d\cos\theta_t = \sigma(e^+e^- \rightarrow t\bar{t}), \end{aligned} \quad (15)$$

which is the normalization of the cross-section.

2.2. Angular spectrum of the bottom quark

It is convenient to define the angular distribution of the bottom quark in the coordinate system shown in Fig. 1 (right). In this system the polar angle of the b quark is determined with respect to the direction of the electron beam which is parallel to the OZ axis. The b -quark momentum is defined by the polar angle θ_b and the azimuthal angle ϕ_b .

The system in Fig. 1 (right) is obtained from the system in Fig. 1 (left) by the clockwise rotation around the OY' axis on the angle θ_t , so that

$$\begin{pmatrix} x \\ y \\ z \end{pmatrix} = \begin{pmatrix} \cos\theta_t & 0 & -\sin\theta_t \\ 0 & 1 & 0 \\ \sin\theta_t & 0 & \cos\theta_t \end{pmatrix} \begin{pmatrix} x' \\ y' \\ z' \end{pmatrix}, \quad (16)$$

where x', y', z' are the primary non-rotated axes and x, y, z are the rotated ones. The four-momenta of the particles and the polarization vector take the form

$$\begin{aligned} k^\mu &= E_t(1, 0, 0, 1), \\ p_t^\mu &= E_t(1, -V \sin\theta_t, 0, V \cos\theta_t), \\ p_b^\mu &= E_b(1, \sin\theta_b \cos\phi_b, \sin\theta_b \sin\phi_b, \cos\theta_b), \\ a^\mu &= (\gamma V P_{z'}, P_{x'} \cos\theta_t - \gamma P_{z'} \sin\theta_t, P_{y'}, P_{x'} \sin\theta_t + \gamma P_{z'} \cos\theta_t), \end{aligned} \quad (17)$$

and for the scalar product $a \cdot p_b$ in (11) we find

$$\begin{aligned} a \cdot p_b &= -E_b [P_{x'} (\cos \theta_t \sin \theta_b \cos \phi_b + \sin \theta_t \cos \theta_b) \\ &\quad + P_{y'} \sin \theta_b \sin \phi_b - P_{z'} \gamma (V - \cos \Theta_{\vec{p}_t \vec{p}_b})], \quad (18) \\ \cos \Theta_{\vec{p}_t \vec{p}_b} &\equiv \cos \theta_t \cos \theta_b - \sin \theta_t \sin \theta_b \cos \phi_b. \end{aligned}$$

Performing integration in (11) over the energy E_b and the azimuthal angle ϕ_b , we obtain the cross-section as a function of the polar angle of the bottom quark

$$\begin{aligned} &\frac{d\sigma(e^+e^- \rightarrow bW^+\bar{t})}{d\cos\theta_b} \\ &= \int_{-1}^{+1} d\cos\theta_t \frac{d\sigma(e^+e^- \rightarrow t\bar{t}; 0)}{d\cos\theta_t} \int_0^{2\pi} \frac{d\phi_b}{(1 - V \cos \Theta_{\vec{p}_t \vec{p}_b})^2} \\ &\quad \times \frac{1}{4\pi\gamma^2} \left[1 + \alpha_b \frac{P_{x'}(\theta_t) (\cos \theta_t \sin \theta_b \cos \phi_b + \sin \theta_t \cos \theta_b)}{\gamma (1 - V \cos \Theta_{\vec{p}_t \vec{p}_b})} \right. \\ &\quad \left. + \alpha_b \frac{P_{y'}(\theta_t) \sin \theta_b \sin \phi_b - P_{z'}(\theta_t) \gamma (V - \cos \Theta_{\vec{p}_t \vec{p}_b})}{\gamma (1 - V \cos \Theta_{\vec{p}_t \vec{p}_b})} \right]. \quad (19) \end{aligned}$$

The normalization of this cross-section is

$$\int_{-1}^{+1} \frac{d\sigma(e^+e^- \rightarrow bW^+\bar{t})}{d\cos\theta_b} d\cos\theta_b = \sigma(e^+e^- \rightarrow t\bar{t}; 0). \quad (20)$$

3. Results of calculation and discussion

3.1. cross-sections

The considered process on the tree level is described by the Feynman diagrams in Fig. 2. We start with description of this process in the framework of the SM without radiative corrections (RCs) to the vertices $\gamma t\bar{t}$ and $Zt\bar{t}$, that corresponds to $\kappa = \kappa_z = 0$. Then we add RC in the SM by choosing nonzero values of κ and κ_z , and finally include anomalous couplings of quarks with the photon and Z boson related to the BSM physics. Thus the structure of the $\gamma t\bar{t}$ and $Zt\bar{t}$ vertices is chosen in the form

$$\Gamma_{\gamma t\bar{t}}^\mu = -ie \left[Q_t \gamma^\mu + i \frac{\sigma^{\mu\nu} q_\nu}{2m_t} (\kappa + i\tilde{\kappa}\gamma_5) \right] \equiv -ie V_{\gamma t\bar{t}}^\mu, \quad (21)$$

$$\begin{aligned} \Gamma_{Zt\bar{t}}^\mu &= -i \frac{g}{2\cos\theta_W} \left[\gamma^\mu (v_t - a_t\gamma_5) + i \frac{\sigma^{\mu\nu} q_\nu}{2m_t} (\kappa_z + i\tilde{\kappa}_z\gamma_5) \right] \\ &\equiv -i \frac{g}{2\cos\theta_W} V_{Zt\bar{t}}^\mu, \quad (22) \end{aligned}$$

where e is the positron charge, $g = e/\sin\theta_W$ with θ_W denoting the weak mixing angle, $Q_t = 2/3$, $v_t = 1/2 - 4/3\sin^2\theta_W$, $a_t = 1/2$, and $q^\nu = k^\nu + k'^\nu$ is the four-momentum of the intermediate photon (Z boson). In the following we neglect the terms in (21) and (22) proportional to $\tilde{\kappa}$ and $\tilde{\kappa}_z$ responsible for the CP violation, and keep only the couplings κ and κ_z related respectively to the anomalous magnetic and anomalous weak-magnetic dipole moments of the t quark. For details on

relation of these couplings to the Wilson coefficients in the EFT Lagrangian and some constraints on their values see Ref. 7.

RC in the SM to the $\gamma t\bar{t}$ and $Zt\bar{t}$ vertices are contained in Eqs. (21), (22) if one chooses the corresponding values, κ_{RC} and $\kappa_{z,RC}$. In this work we do not take into account other RC to the $e^+e^- \rightarrow t\bar{t}$ reaction, as well as to the $t \rightarrow bW^+$ decay. For $e^+e^- \rightarrow t\bar{t}$, certain RC have been studied in Refs. 20–24.

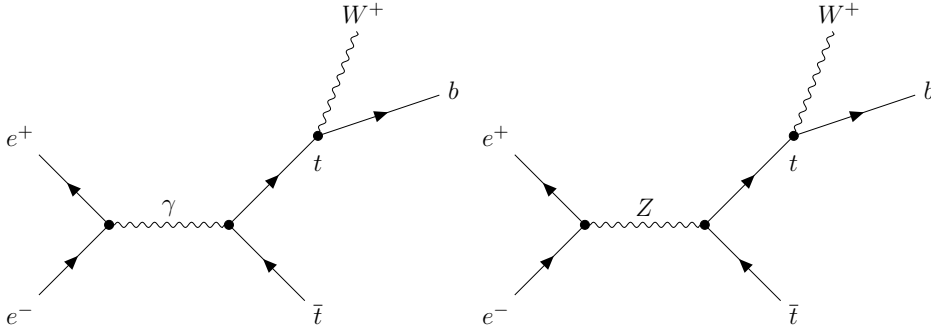


Fig. 2. Feynman diagrams for $e^+e^- \rightarrow t\bar{t} \rightarrow bW^+t\bar{t}$ reaction. The vertices $\gamma t\bar{t}$ and $Zt\bar{t}$ can include RC and BSM couplings.

In general, the diagrams in Fig. 2 do not satisfy the condition of gauge invariance, and additional tree-level diagrams are needed to satisfy the gauge invariance.^{25–27} In the approach used in the present paper, it is assumed following^{8,17} that the intermediate t quark, decaying to b quark and W boson, is on its mass shell. This assumption is realized via the narrow-width approximation (NWA) which is used in derivation of Eqs. (1) and (2). In Appendix A we show explicitly that in this approach the photon-exchange diagram in Fig. 2 satisfies the gauge invariance.

The calculated cross-section (13) is shown in Fig. 3 for the e^+e^- energy 380 GeV. The energy of the bottom quark lies in the interval $43.7 \text{ GeV} \leq E_b \leq 105.3 \text{ GeV}$. We present two variants of the calculation: the first one corresponds to neglect of the t -quark polarization, $\vec{P} = 0$ (called “depolarized” process), and the second one corresponds to inclusion of the polarization, $\vec{P} \neq 0$ (called “polarized” process). The corresponding curves in Fig. 3 (dashed and solid) cross at the energy $\hat{E}_b = \gamma p_b^0 = (E_+ + E_-)/2 = 74.5 \text{ GeV}$.

In Fig. 3 we also show cross-section for several values of the couplings κ and κ_z . Note that, firstly, the cross-section varies considerably with the couplings and, secondly, the difference between the polarized and depolarized cases is similar to the SM calculation, but the slope of the solid straight lines depends on the couplings. This is demonstrated in Table 1.

The values of the couplings in Fig. 3 and Table 1 are chosen as in Ref. 7. Namely, in the first line the values correspond to the SM without RC ($\kappa = \kappa_z = 0$), while the second line includes RC in the SM in Eqs. (21) and (22) ($\kappa_{RC} = 0.02$,

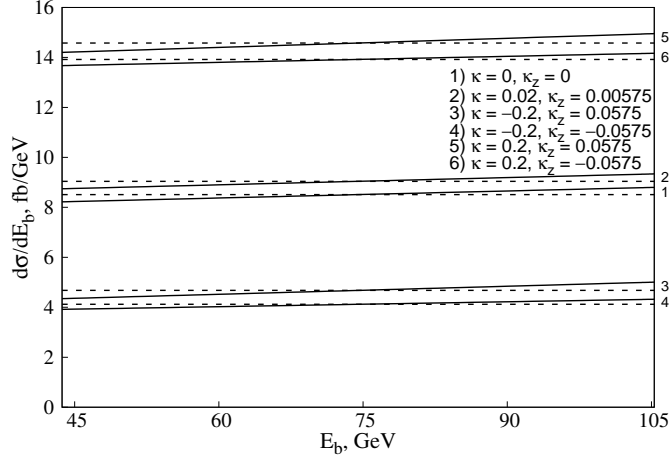


Fig. 3. The cross-section of the process $e^+ e^- \rightarrow b W^+ \bar{t}$ as a function of the bottom-quark energy: (1) in the SM without RC, (2) in the SM with RC, and (3)-(6) beyond the SM. The $e^+ e^-$ energy is $\sqrt{s} = 380$ GeV. Solid (dashed) curves correspond to the polarized (depolarized) process.

$\kappa_{z,RC} = 0.00575$). The latter were evaluated in Ref. 28 to the two loops in QCD and to the lowest order in electroweak couplings. The other values in Fig. 3 and Table 1 are chosen ten times bigger than κ_{RC} and $\kappa_{z,RC}$, as a conservative estimate. Since the sign of the BSM couplings is not known, the negative signs are also included. It is seen that the slope of the energy distribution depends on the BSM couplings, although the dependence is weak, at least for the considered moderate values of κ and κ_z .

Table 1. The slope of the cross-section $d\sigma(e^+ e^- \rightarrow b W^+ \bar{t})/dE_b$ for various couplings κ, κ_z . The $e^+ e^-$ invariant energy is 380 GeV.

κ	κ_z	slope, 10^{-3} fb/GeV ²
0.0	0.0	9.4
0.02	0.00575	9.7
0.2	0.0575	12.2
0.2	-0.0575	8.0
-0.2	0.0575	10.7
-0.2	-0.0575	6.6

In Fig. 4 we show the angular spectrum of the b quark (19). One can notice that in all calculations the solid and dashed curves cross at the point close to the angle $\tilde{\theta} \approx \pi/2$. As can also be seen from Fig. 4, the difference between the polarized and depolarized processes is more pronounced than the corresponding effect in the energy dependence in Fig. 3. Apparently the angular dependence is more sensitive to the top-quark polarization.

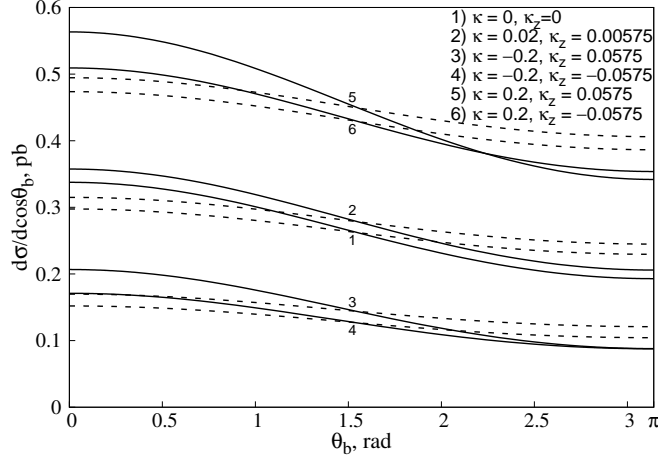


Fig. 4. The cross-section of the process $e^+e^- \rightarrow bW^+\bar{t}$ as a function of the b -quark polar angle: (1) in the SM without RC, (2) in the SM with RC, and (3)-(6) beyond the SM. Solid (dashed) curves correspond to the polarized (depolarized) process.

It is of interest to plot the energy and angular normalized distributions

$$W(E_b) \equiv \frac{1}{\sigma(e^+e^- \rightarrow t\bar{t})} \frac{d\sigma(e^+e^- \rightarrow bW^+\bar{t})}{dE_b}, \quad (23)$$

$$W(\theta_b) \equiv \frac{1}{\sigma(e^+e^- \rightarrow t\bar{t})} \frac{d\sigma(e^+e^- \rightarrow bW^+\bar{t})}{d\cos\theta_b}, \quad (24)$$

which satisfy the normalization

$$\int_{E_-}^{E_+} W(E_b) dE_b = \int_0^\pi W(\theta_b) \sin\theta_b d\theta_b = 1. \quad (25)$$

These distributions are shown in Fig. 5. It is seen that for the energy distributions in Fig. 5 (left), all the curves cross at the energy $\tilde{E}_b = \gamma p_b^0$. This behavior follows from Eq. (13), in particular, the couplings κ and κ_z contribute only to the polarization-dependent part proportional to $E_b - \tilde{E}_b$ which vanishes at $E_b = \tilde{E}_b$. The value of the distribution at the crossing point is $W(\tilde{E}_b) = (E_+ - E_-)^{-1} = (2V\tilde{E}_b)^{-1}$, which is 0.0162 GeV^{-1} at the e^+e^- energy 380 GeV.

The angular distribution in Fig. 5 (right) has somewhat different features which follow from Eq. (19). The couplings κ and κ_z enter both polarization-independent and polarization-dependent parts of the distribution. All the curves cross at the angle $\tilde{\theta}_b \approx \pi/2$, and the value at the crossing point is $W(\tilde{\theta}_b) = 1/2$ independently of the e^+e^- energy. It is also seen that the angular distribution is more sensitive to values of κ and κ_z than the energy distribution.

These simple properties of the energy and angular normalized distributions make them convenient observables for future experimental studies.

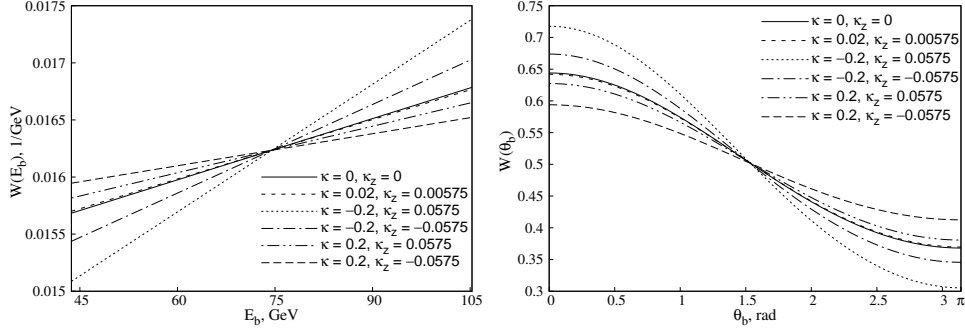


Fig. 5. Energy (left panel) and angular (right panel) normalized distributions of the bottom quark at various values of the couplings κ , κ_z . The e^+e^- energy is 380 GeV. All curves are calculated for the polarized process.

3.2. Asymmetries

Other important observables, sensitive to the BSM couplings, are the asymmetries of the cross-sections. In particular, for the cross-section in Eq. (13) one can define the energy asymmetry

$$\mathcal{A}_E = \left(\int_{\tilde{E}_b}^{E_+} - \int_{E_-}^{\tilde{E}_b} \right) dE_b \frac{d\sigma(e^+e^- \rightarrow bW^+\bar{t})}{dE_b} \bigg/ \int_{E_-}^{E_+} dE_b \frac{d\sigma(e^+e^- \rightarrow bW^+\bar{t})}{dE_b}, \quad (26)$$

where the energy $\tilde{E}_b = \gamma p_b^0$. This energy is determined by the e^+e^- energy \sqrt{s} .

For the cross-section in Eq. (19) the forward backward (FB) asymmetry can be defined as follows

$$\mathcal{A}_{FB} = \left(\int_0^{+1} - \int_{-1}^0 \right) dz \frac{d\sigma(e^+e^- \rightarrow bW^+\bar{t})}{dz} \bigg/ \int_{-1}^{+1} dz \frac{d\sigma(e^+e^- \rightarrow bW^+\bar{t})}{dz} \quad (27)$$

with $z \equiv \cos\theta_b$. Due to the normalizations (15) and (20) the denominators of asymmetries (26) and (27) are fixed by the total $e^+e^- \rightarrow t\bar{t}$ cross-section.

The calculated asymmetries are presented in Table 2. The values of the BSM couplings are chosen as in Table 1. It is seen that for certain coupling constants the energy asymmetry reaches a few percent, and the angular asymmetry takes quite sizable values 10–20% that could be accessible in future experiments.

It is of interest to study dependence of the asymmetries on the e^+e^- energy. The dependence of \mathcal{A}_E on \sqrt{s} is plotted in Fig. 6, and the corresponding dependence of \mathcal{A}_{FB} is plotted in Fig. 7.

As follows from Fig. 6, the energy asymmetry in the SM rises up to the energy ~ 1 TeV and then stays almost constant, while the asymmetry beyond the SM has another trend – there is a wide maximum at the energy $\sqrt{s} \sim 650$ –850 GeV and then it decreases. This behavior can be of interest for the experimental studies at the CLIC, during the next stages of its run, in which the energy is planned to be 1.5 TeV (the 2nd construction stage) and 3 TeV (the 3rd construction stage) with

Table 2. The asymmetries \mathcal{A}_E and \mathcal{A}_{FB} in % for various values of the couplings κ and κ_z at the e^+e^- energy 380 GeV.

κ	κ_z	\mathcal{A}_E	\mathcal{A}_{FB}
0.0	0.0	1.7	14.0
0.02	0.00575	1.6	14.0
0.2	0.0575	1.3	12.0
0.2	-0.0575	0.9	9.0
-0.2	0.0575	4.0	21.0
-0.2	-0.0575	2.0	16.0

the expected integrated luminosities of 2.5 ab^{-1} and 5 ab^{-1} , respectively.

Somewhat similar behavior is observed for the angular asymmetry in Fig. 7, though the values of \mathcal{A}_{FB} are an order of magnitude larger than the values of \mathcal{A}_E .

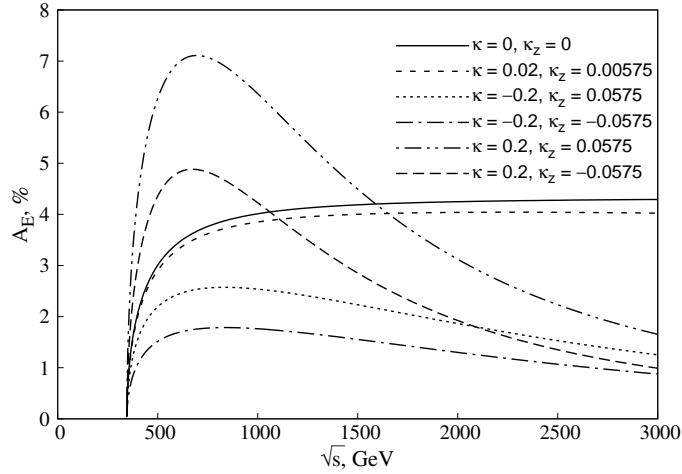


Fig. 6. The energy asymmetry as a function of \sqrt{s} for various values of the couplings.

Finally, we briefly address the equivalence of the two methods of calculation of the cross-section mentioned in the beginning of Sec. 2. One has to check the equivalence of Eqs. (1) and (2), though formally they look differently. To calculate the cross-section using Eq. (2), we evaluate the $e^+e^- \rightarrow t\bar{t}$ differential cross-section with the polarization density matrix of the top quark

$$u(p_t, m_t) \bar{u}(p_t, m_t) = \frac{1}{2} (\not{p}_t + m_t) (1 + \gamma^5 \not{\eta}) \quad (28)$$

with $\not{p}_t = \gamma \cdot p_t$, $\not{\eta} = \gamma \cdot n$ and the four-vector n^μ given in (3). Note that in the top-quark rest frame $n_R^\mu = (0, \alpha_b \vec{n}_{b,R})$.

Our explicit calculation of the differential cross-sections in Eq. (13) and Eq. (19) shows that equations (1) and (2) lead to the identical results, as expected.

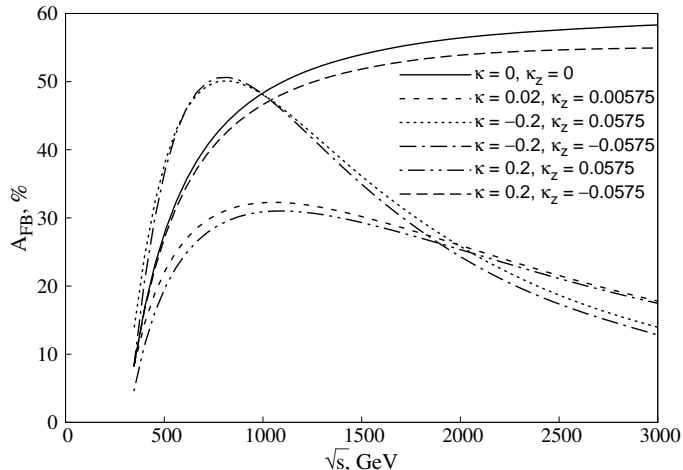


Fig. 7. The angular asymmetry as a function of \sqrt{s} for various values of the couplings.

4. Conclusions

We studied the spectra of the bottom quark from the decay of the top quark, $t \rightarrow bW^+$, produced in the electron-positron annihilation. The formalism used in calculation is based on the method of Ref. 17. The cross-sections of the process $e^+e^- \rightarrow t\bar{t} \rightarrow bW^+\bar{t}$, as functions of the b -quark energy and angle with respect to the direction of the electron beam, are derived and calculated. In the calculation the e^+e^- energy $\sqrt{s} = 380$ GeV corresponding to the first construction stage of the CLIC, was chosen.

We investigated the influence of the top-quark polarization, which arises in the $e^+e^- \rightarrow t\bar{t}$ reaction, on the energy and angular spectra of the bottom quark. In general, the difference between the cross-sections for the polarized and unpolarized top quark is not too big, the effect is of the order of 10%. The angular spectrum turns out to be more sensitive to the top-quark polarization than the energy spectrum.

It is shown that the cross-section of the $e^+e^- \rightarrow bW^+\bar{t}$ reaction strongly depends on values of the $\gamma t\bar{t}$ and $Zt\bar{t}$ anomalous couplings κ and κ_z . These couplings beyond the SM can take quite sizable values, and we studied how the energy and angular spectra of the b quark depend on κ and κ_z . It follows from the calculations that the BSM effects can be quite important and perspective for studying the top quark properties.

Several observables sensitive to these couplings were considered, namely, the energy and angular normalized distributions, and the energy and angular asymmetries. In particular, the angular asymmetry \mathcal{A}_{FB} at $\sqrt{s} = 380$ GeV reaches 10–20%, that can possibly be accessible in future experiments. We also investigated dependence of these asymmetries on the invariant e^+e^- energy up to $\sqrt{s} = 3$ TeV. An interesting trend is observed – for the couplings beyond the SM these asymmetries

have a maximum at the energy $\sqrt{s} = 650\text{--}850$ GeV and then they decrease, while in the SM the asymmetries slowly rise with e^+e^- energy and reach $\sim 4\%$ for the energy asymmetry and $\sim 60\%$ for the angular asymmetry. This behavior can be of interest for future studies at the CLIC at the next stages of its run, and for other e^+e^- colliders.

Although the consideration in the paper was performed for the unpolarized electron and positron, the present method can easily be extended to the case of the polarized electron and positron beams. The next step in future can also be the study of the joint distributions of b and \bar{b} quarks from decays of the top quark and antiquark.

Acknowledgments

This work was partially conducted in the scope of the IDEATE International Associated Laboratory (LIA). The authors acknowledge partial support by the National Academy of Sciences of Ukraine via the program ‘‘Support for the development of priority areas of scientific research’’ (6541230).

Appendix A. Gauge Invariance of Matrix Element of the $e^+e^- \rightarrow t\bar{t} \rightarrow bW^+\bar{t}$ Process

In this Appendix we prove the gauge invariance of matrix element for the photon-exchange diagram in Fig. 2 in the narrow-width approximation (NWA). This approximation lies in the derivation of Eqs. (1) and (2) which are used in the calculation.

This corresponding matrix element can be written as

$$\begin{aligned} \mathcal{M} &= \frac{1}{q^2} \ell_\mu J^\mu, \quad \ell_\mu = e \bar{v}(k') \gamma_\mu u(k), \\ J^\mu &= \frac{eg}{2\sqrt{2}} \frac{1}{p_{\bar{t}}^2 - m_{\bar{t}}^2 + im_{\bar{t}}\Gamma_{\bar{t}}} I^\mu, \\ I^\mu &= \bar{u}(p_b) \not{\epsilon}^*(p_W) (1 - \gamma_5) (\not{p}_t + m_t) V_{\gamma\bar{t}}^\mu v(p_{\bar{t}}) \end{aligned} \quad (\text{A.1})$$

with the energy momentum conservation $k + k' \equiv q = p_t + p_{\bar{t}} = p_b + p_W + p_{\bar{t}}$, $\not{\epsilon}^*(p_W) = \gamma^\alpha \epsilon_\alpha^*(p_W)$, where $\epsilon(p_W)$ is the polarization four-vector of the W boson. The spinors of the electron and positron are $u(k)$ and $v(k')$, and those of the bottom quark and top antiquark are $u(p_b)$ and $v(p_{\bar{t}})$. In Eq. A.1 the propagator of the intermediate top quark is taken in the form

$$S(p_t) = \frac{\not{p}_t + m_t}{p_t^2 - m_t^2 + im_t\Gamma_t} \quad (\text{A.2})$$

with the top quark total decay width Γ_t .

The $\gamma t\bar{t}$ vertex $V_{\gamma t\bar{t}}^\mu$ for the on-mass-shell quarks can be chosen in the general form²⁹

$$V_{\gamma t\bar{t}}^\mu = F_1(q^2)\gamma^\mu + i\frac{\sigma^{\mu\alpha}q_\alpha}{2m_t}[F_2(q^2) - i\gamma_5 F_3(q^2)]. \quad (\text{A.3})$$

With the proper normalization of the form factors $F_{1,2,3}(q^2)$ at $q^2 = 0$, Eq. (A.3) reduces to the vertex in Eq. (21).

After squaring the matrix element we get

$$|\mathcal{M}|^2 = \frac{e^4 g^2}{8q^4 [(p_t^2 - m_t^2)^2 + m_t^2 \Gamma_t^2]} \ell_\mu \ell_\nu^* W^{\mu\nu}, \quad W^{\mu\nu} = I^\mu I^{\nu*}. \quad (\text{A.4})$$

In the NWA one applies the relation (see, for example Refs. 8,17)

$$\frac{1}{(p_t^2 - m_t^2)^2 + m_t^2 \Gamma_t^2} \approx \frac{\pi}{m_t \Gamma_t} \delta(p_t^2 - m_t^2), \quad (\text{A.5})$$

valid for $\Gamma_t \ll m_t$. Note that accuracy of the NWA has been studied in various processes.^{30–33}

Let us now check the gauge invariance. We use the condition $q_\mu V_{\gamma t\bar{t}}^\mu = F_1(q^2)\not{q} = F_1(q^2)(\not{p}_t + \not{p}_{\bar{t}})$ and obtain

$$q_\mu W^{\mu\nu} = F_1(q^2)(p_t^2 - m_t^2) \bar{u}(p_b) \not{\epsilon}^*(p_W)(1 - \gamma_5)v(p_{\bar{t}}) I^{\nu*}, \quad (\text{A.6})$$

and therefore in view of (A.4) and (A.5), $q_\mu W^{\mu\nu} = 0$. Clearly, $q_\nu W^{\mu\nu} = 0$ as well.

We emphasize that this result is a consequence of the NWA which implies that the intermediate top quark is on mass shell, $p_t^2 = m_t^2$. Otherwise the gauge invariance would be violated, and additional tree-level diagrams discussed in Refs. 25–27 would be needed to restore the gauge invariance.

It is interesting to note, that in the present approach the gauge invariance holds for arbitrary form factors $F_{1,2,3}(q^2)$ which can include radiative corrections and effects beyond the SM.

References

1. T. Behnke, J. E. Brau, B. Foster, J. Fuster, M. Harrison, J. M. Paterson, M. Peskin, M. Stanitzki, N. Walker and H. Yamamoto [arXiv:1306.6327 \[physics.acc-ph\]](#), doi:10.2172/1347945.
2. M. Aicheler, P. Burrows, M. Draper, T. Garvey, P. Lebrun, K. Peach, N. Phinney, H. Schmickler, D. Schulte and N. Toge doi:10.5170/CERN-2012-007.
3. CLICdp Collaboration (A. F. Zarnecki), *PoS ALPS2019* [arXiv:1908.04671 \[hep-ex\]](#).
4. CLICdp, ILD concept group Collaboration (A. F. Zarnecki), *PoS CORFU2019*, 037 [arXiv:2004.14628 \[hep-ph\]](#), doi:10.22323/1.376.0037.
5. Linear Collider Collaboration (L. Evans and S. Michizono) [arXiv:1711.00568 \[physics.acc-ph\]](#).
6. CLIC, CLICdp Collaboration (M. J. Boland *et al.*) [arXiv:1608.07537 \[physics.acc-ph\]](#), doi:10.5170/CERN-2016-004.
7. I. V. Truten and A. Y. Korchin, *Int. J. Mod. Phys. A* **34**, 1950067 [arXiv:1902.09911 \[hep-ph\]](#), doi:10.1142/S0217751X19500672.

8. T. Arens and L. M. Sehgal, *Phys. Rev. D* **50**, 4372 doi:10.1103/PhysRevD.50.4372.
9. T. Arens and L. M. Sehgal, *Nucl. Phys. B* **393**, 46 doi:10.1016/0550-3213(93)90236-I.
10. B. Grzadkowski and Z. Hioki, *Nucl. Phys. B* **484**, 17 [arXiv:hep-ph/9604301](#), doi:10.1016/S0550-3213(96)00602-5.
11. B. Grzadkowski and Z. Hioki, *Phys. Lett. B* **529**, 82 [arXiv:hep-ph/0112361](#), doi:10.1016/S0370-2693(02)01250-9.
12. E. Christova, *Int. J. Mod. Phys. A* **14**, 1 [arXiv:hep-ph/9809290](#), doi:10.1142/S0217751X99002451.
13. A. Bartl, E. Christova and W. Majerotto, *Nucl. Phys. B* **460**, 235 [arXiv:hep-ph/9507445](#), doi:10.1016/0550-3213(95)00635-4, [Erratum: *Nucl.Phys.B* 465, 365–365 (1996)].
14. A. Bartl, E. Christova, T. Gajdosik and W. Majerotto, *Phys. Rev. D* **58**, 074007 [arXiv:hep-ph/9802352](#), doi:10.1103/PhysRevD.58.074007.
15. A. Bartl, E. Christova, T. Gajdosik and W. Majerotto, *Phys. Rev. D* **59**, 077503 [arXiv:hep-ph/9803426](#), doi:10.1103/PhysRevD.59.077503.
16. J. A. Aguilar-Saavedra, *Nucl. Phys. B* **812**, 181 [arXiv:0811.3842 \[hep-ph\]](#), doi:10.1016/j.nuclphysb.2008.12.012.
17. S. Kawasaki, T. Shirafuji and S. Y. Tsai, *Prog. Theor. Phys.* **49**, 1656 doi:10.1143/PTP.49.1656.
18. E. Christova and D. Draganov, *Phys. Lett. B* **434**, 373 [arXiv:hep-ph/9710225](#), doi:10.1016/S0370-2693(98)00630-3.
19. V. B. Berestetskii, E. M. Lifshitz and L. P. Pitaevskii, *Quantum Electrodynamics*, Course of Theoretical Physics, Vol. 4 (Pergamon Press, Oxford).
20. J. G. Korner, A. Pilaftsis and M. M. Tung, *Z. Phys. C* **63**, 575 doi:10.1007/bf01557623.
21. S. Groote, J. G. Korner and M. M. Tung, *Z. Phys. C* **70**, 281 [arXiv:hep-ph/9507222](#), doi:10.1007/s002880050105.
22. S. Groote and J. G. Korner, *Z. Phys. C* **72**, 255 [arXiv:hep-ph/9508399](#), doi:10.1007/s002880050243, [Erratum: *Z.Phys.C* 70, 531E (2010)].
23. J. B. Stav and H. A. Olsen, *Phys. Rev. D* **54**, 817 doi:10.1103/PhysRevD.54.817.
24. H. A. Olsen and J. B. Stav, *Phys. Rev. D* **56**, 407 doi:10.1103/PhysRevD.56.407.
25. E. Boos and T. Ohl, *Phys. Rev. Lett.* **83**, 480 [arXiv:hep-ph/9903357](#), doi:10.1103/PhysRevLett.83.480.
26. E. Boos, M. Dubinin, A. Pukhov, M. Sachwitz and H. Schreiber, *Eur. Phys. J. C* **21**, 81 [arXiv:hep-ph/0104279](#), doi:10.1007/s100520100733.
27. E. Boos and L. Dudko, *Int. J. Mod. Phys. A* **27**, 1230026 [arXiv:1211.7146 \[hep-ph\]](#), doi:10.1142/S0217751X12300268.
28. W. Bernreuther, R. Bonciani, T. Gehrmann, R. Heinesch, T. Leineweber, P. Mastrolia and E. Remiddi, *Phys. Rev. Lett.* **95**, 261802 [arXiv:hep-ph/0509341](#), doi:10.1103/PhysRevLett.95.261802.
29. W. Hollik, J. I. Illana, S. Rigolin, C. Schappacher and D. Stockinger, *Nucl. Phys. B* **551**, 3 [arXiv:hep-ph/9812298](#), doi:10.1016/S0550-3213(99)00396-X.
30. N. Achasov and V. Gubin, *Phys. Lett. B* **363**, 106 doi:10.1016/0370-2693(95)01197-X.
31. D. Berdine, N. Kauer and D. Rainwater, *Phys. Rev. Lett.* **99**, 111601 [arXiv:hep-ph/0703058](#), doi:10.1103/PhysRevLett.99.111601.
32. C. Uhlemann and N. Kauer, *Nucl. Phys. B* **814**, 195 [arXiv:0807.4112 \[hep-ph\]](#), doi:10.1016/j.nuclphysb.2009.01.022.
33. T. V. Zagoskin and A. Y. Korchin, *J. Exp. Theor. Phys.* **122**, 663 [arXiv:1504.07187 \[hep-ph\]](#), doi:10.1134/S1063776116020229.